



Cite this: *Phys. Chem. Chem. Phys.*,
2015, 17, 25799

Structural characterization of gas-phase cysteine and cysteine methyl ester complexes with zinc and cadmium dications by infrared multiple photon dissociation spectroscopy†

Rebecca A. Coates,^a Christopher P. McNary,^a Georgia C. Boles,^a Giel Berden,^b Jos Oomens^{bc} and P. B. Armentrout^{*a}

Structural characterization of gas-phase ions of cysteine (Cys) and cysteine methyl ester (CysOMe) complexed to zinc and cadmium is investigated by infrared multiple photon dissociation (IRMPD) action spectroscopy using a free electron laser in combination with density functional theory calculations. IRMPD spectra are measured for $[\text{Zn}(\text{Cys}-\text{H})]^+$, $[\text{Cd}(\text{Cys}-\text{H})]^+$, $[\text{Zn}(\text{CysOMe}-\text{H})]^+$, $[\text{Cd}(\text{CysOMe}-\text{H})]^+$ and $\text{CdCl}^+(\text{CysOMe})$ and are accompanied by quantum mechanical calculations of the predicted linear absorption spectra at the B3LYP/6-311+G(d,p) (Zn^{2+} complexes) and B3LYP/def2TZVP levels (Cd^{2+} complexes). On the basis of these experiments and calculations, the conformation that best reproduces the IRMPD spectra for the complexes of the deprotonated amino acids, $[\text{M}(\text{Cys}-\text{H})]^+$ and $[\text{M}(\text{CysOMe}-\text{H})]^+$, is a charge-solvated (CS) tridentate structure where the metal dication binds to the amine and carbonyl groups of the amino acid backbone and the deprotonated sulfur atom of the side chain, $[\text{N},\text{CO},\text{S}^-]$. The intact amino acid complex, $\text{CdCl}^+(\text{CysOMe})$ binds in the equivalent motif $[\text{N},\text{CO},\text{S}]$. These binding motifs are in agreement with the predicted ground structures of these complexes at the B3LYP, B3LYP-GD3BJ (with empirical dispersion corrections), B3P86, and MP2(full) levels.

Received 13th March 2015,
Accepted 8th April 2015

DOI: 10.1039/c5cp01500f

www.rsc.org/pccp

Introduction

A large number of proteins have been found to exhibit metal-dependent transcription regulation activities and contain cysteine-rich sequence motifs capable of coordinating Zn^{2+} ions.¹ Included in these are zinc finger proteins, metalloproteins that utilize zinc ions for structural integrity.² These zinc finger proteins are characterized by divalent Zn^{2+} centers directly coordinated to amino acid residues, most commonly binding as $\text{Zn}(\text{Cys})_{4-n}(\text{His})_n$, where $n = 0-2$.³ Zinc finger proteins are active in transcription factors as well as in DNA-repair of enzymes. Competition from toxic metal ions that replace the essential zinc ion center has been observed^{4,5} and has a profound effect on the protein's structure and function, essentially deactivating it.

Toxic metals that have high affinities for thiol groups make cysteine containing zinc finger proteins particularly susceptible to Zn^{2+} replacement. This includes cadmium, its group 12 congener, even in low concentrations.⁶ The mechanisms of cadmium toxicity is not well understood, although cadmium is known to target thiol groups in proteins.⁷ The mechanism for zinc finger protein inactivation by toxic metal replacement is presumed to involve structural changes of the coordinating amino acid residues. Investigating these complexes in isolation at the fundamental level may be beneficial to unveiling structural evidence for how these metals coordinate with the relevant amino acid residues. Theoretical investigations by Russo *et al.* of the interactions of cysteine with Cu^{2+} , Zn^{2+} , Cd^{2+} , and Hg^{2+} found that zinc and cadmium both form stable complexes by coordination of the metal to cysteine in a tridentate binding pattern involving the amino nitrogen, carbonyl oxygen, and side-chain sulfur.⁸ Similarly, quantum chemical studies by Mori *et al.*⁹ examined the interactions of Hg^{2+} , Cd^{2+} , and Zn^{2+} with deprotonated cysteine either microsolvated by one or two water molecules or using a polarized continuum model. For one water ligand, they found a similar tridentate motif, where deprotonation occurs at the thiol. When placed in solution, the Zn complex retains the tridentate binding motif, whereas the Cd complex prefers the bidentate conformation. For two waters (gas-phase or in solution),

^a Department of Chemistry, University of Utah, Salt Lake City, UT 84112, USA.
E-mail: armentrout@chem.utah.edu

^b Radboud University, Institute for Molecules and Materials, FELIX Laboratory, Toernooiveld 7, NL-6525ED Nijmegen, The Netherlands

^c van't Hoff Institute for Molecular Sciences, University of Amsterdam, Amsterdam, The Netherlands

† Electronic supplementary information (ESI) available: Relative 0 K enthalpies and 298 K free energies for all conformers of all complexes studied here calculated at the B3LYP, B3LYP-GD3BJ, B3P86, and MP2(full) levels of theory with 6-311+G(2d,2p) and def2TZVPP basis sets are given in Table S1. This material is available free of charge via the Internet see DOI: 10.1039/c5cp01500f

a bidentate chelation by the amino nitrogen and deprotonated sulfur is preferred for both Zn and Cd. In the context of hydration, we have previously studied the hydration energies of both Zn^{2+} and Cd^{2+} ,^{10,11} finding that Zn^{2+} binds more strongly than Cd^{2+} by $\sim 8 \text{ kJ mol}^{-1}$ for six through eight water ligands, but less strongly by $\sim 5 \text{ kJ mol}^{-1}$ for the ninth and tenth water ligands. It should be realized that the solvated environment may be relevant to the delivery of these metal ions to the zinc finger sites, but in the protein, the metal ion remains unsolvated by water.

In previous experimental work, Bohme and coworkers examined the collision-induced dissociation of Zn^{2+} bound to 12-residue peptides containing either two cysteines and two histidines (CCHH and CHCH) or four cysteines (CCCC).¹² They concluded that zinc binds to both residues but prefers binding to histidine. No specific details of the binding site for these residues could be provided. Previously, our group has examined complexes of the single amino acid histidine (His) with Zn^{2+} and Cd^{2+} using infrared multiple photon dissociation (IRMPD) action spectroscopy.¹³ In these cases, the simple $\text{M}^{2+}(\text{His})$ complexes were not generated directly by electrospray ionization. Thus the interactions of the metal ions with histidine were mimicked by examining the $\text{CdCl}^+(\text{His})$ and $[\text{M}(\text{His-H})]^+$ systems. Structures for these systems were determined definitively using IRMPD spectroscopy and quantum chemical calculations, finding that the metal ions bind to His in a tridentate conformation by attaching to a carboxylate oxygen, the backbone amino group (N), and the imidazole side-chain nitrogen (N_π). Deprotonation in the $[\text{M}(\text{His-H})]^+$ complexes was found unequivocally to be at the carboxylic acid for both metals. The present study approaches the metal–cysteine (Cys) binding interaction similarly with a systematic structural investigation using IRMPD action spectroscopy and quantum chemical calculations. Conformations are identified by comparing the experimental IRMPD action spectra to IR spectra derived from quantum chemical calculations at the B3LYP/6-311+G(d,p) (Zn^{2+} complexes) and B3LYP/def2TZVP levels (Cd^{2+} complexes) levels of theory of the low-lying structures of the complexes. In order to definitively ascertain whether structures of these complexes involve deprotonation of the carboxylic acid site, as seen in the His study, metal binding to cysteine methyl ester (CysOMe) is also examined.

Experimental and theoretical methods

Mass spectrometry and IRMPD spectroscopy

Experiments were performed at the FELIX Facility, Radboud University, The Netherlands, using the Free Electron Laser for Infrared eXperiments (FELIX)¹⁴ beam line. A 4.7 T Fourier transform ion cyclotron resonance (FT-ICR) mass spectrometer, described elsewhere,^{15–17} was used to record the IRMPD spectra. The metal–cysteine complex ions were generated using a Micro-mass Z-spray electrospray ionization source. Solutions of 1.0 mM Cys with 1.0 mM zinc nitrate or cadmium chloride in 50:50 MeOH:H₂O solution were used with a flow rate of 3–10 $\mu\text{L min}^{-1}$. Ions generated from the ESI were accumulated in a hexapole trap for 5–7 s before being pulse extracted through a quadrupole

bender and injected into the ICR cell *via* a radiofrequency (rf) octopole ion guide. Ion capturing was affected by electrostatic switching of the dc bias of the octopole to avoid collisional heating of the ions.¹⁵ Once trapped in the ICR cell, the ions are cooled to room temperature and the ion of interest is mass isolated using a stored waveform inverse Fourier transform (SWIFT) excitation pulse^{18,19} and irradiated with FELIX for 3–5 s at a 5 or 10 Hz macropulse repetition rate. At each wavelength, the parent and fragment ion intensities are used to determine the fractional yield, $Y = \Sigma I_F / (I_P + \Sigma I_F)$, where I_P and I_F are the integrated intensities of the parent and fragment ion mass peaks, respectively. The IRMPD spectra are generated by plotting the yield as a function of the wavenumber of the IR radiation.

The ESI source generated $[\text{M}(\text{Cys-H})\text{ACN}]^+$, $[\text{M}(\text{CysOMe-H})\text{ACN}]^+$ and $\text{CdCl}^+(\text{CysOMe})$ directly for $\text{M} = \text{Zn}$ and Cd where ACN = acetonitrile (originally, the ACN was present adventitiously from previous experiments, although in some cases, additional ACN was added to the electrospray solution to enhance intensities of these complexes). The $[\text{M}(\text{Cys-H})]^+$ and $[\text{M}(\text{CysOMe-H})]^+$ species interrogated here were generated by irradiation of their corresponding ACN adduct ions with a 40 W continuous-wave CO₂ laser for 0.2 s and then allowing the resulting ions to cool for an additional 0.1 s before isolation in the FT-ICR and irradiation with the FELIX light.

Computational details

Possible geometries for $\text{Zn}^{2+}(\text{Cys})$ complexes were taken from previously published geometries of $\text{Li}^+(\text{Cys})$ complexes.²⁰ Structures were optimized using density functional theory (DFT) and the Gaussian09 suite of programs²¹ at the B3LYP/6-31G(d) level of theory^{22,23} using the “loose” keyword to utilize a large step size of 0.01 au and rms force constant of 0.0017 to ensure a rapid geometry convergence. These structures were refined by geometry optimization at a B3LYP/6-311+G(d,p) level. From these optimized structures, the Cys residue was deprotonated at likely sites (S, O, or N) yielding $[\text{Zn}(\text{Cys-H})]^+$ structures that were refined again in the loose optimization step. Remaining unique converged structures were then chosen for further geometry optimization and vibrational frequency calculations at the B3LYP/6-311+G(d,p) level of theory. Geometry optimizations utilizing empirical dispersion corrections were also determined at the B3LYP-GD3BJ/6-311+G(d,p) level.²⁴ The $[\text{Cd}(\text{Cys-H})]^+$ complexes went through the same geometry optimization procedure except the def2TZVP basis set was used, where def2TZVP is a size-consistent basis set for all atoms and includes triple- ζ + polarization functions with a small core (28 electron) effective core potential (ECP) on Cd.^{25,26} The def2TZVP basis set and affiliated ECP were obtained from the EMSL basis set exchange.²⁷ Single-point energy calculations were carried out at the B3LYP, B3LYP-GD3BJ, B3P86,²⁸ and MP2(full)²⁹ (where full indicates correlation of all electrons) levels using the 6-311+G(2d,2p) (def2TZVPP) basis sets for Zn (Cd) complexes. Zero point energy (ZPE) corrections scaled by 0.989 were determined in order to provide 0 K relative energies and thermal corrections to free energies at 298 K. For comparison to IRMPD experimental spectra, calculated frequencies were scaled by 0.975, as this factor

leads to good agreement between calculated and experimentally well-resolved peaks and is consistent with previous IRMPD studies of metal–amino acid complexes.^{13,30–34} Calculated vibrational frequencies are broadened using a 15 cm⁻¹ full width at half maximum Gaussian line shape for comparison with experimental spectra.

Results and discussion

Theoretical results

Overview. As described above, low-energy structures of the [M(Cys-H)]⁺, [M(CysOMe-H)]⁺, and CdCl⁺(CysOMe) complexes were optimized at the B3LYP/6-311+G(d,p) level of theory. Table 1 provides relative 298 K Gibbs free energies for the low-energy conformers of [M(Cys-H)]⁺. Relative energies at 0 K with respect to the ground structure (GS) calculated at three different levels of theory are given in Table S1 of the ESI,[†] for low-energy conformations of [M(Cys-H)]⁺, [M(CysOMe-H)]⁺, and CdCl⁺(CysOMe) complexes. Several higher energy isomers of these complexes, although not explicitly discussed here because of their high energies, were also calculated and are included in Table S1 (ESI[†]). Select low-lying conformations of [Zn(Cys-H)]⁺ are shown in Fig. 1. Similar binding modes are found for [Zn(CysOMe-H)]⁺, Cd²⁺ complexes with deprotonated Cys and CysOMe, and CdCl⁺(CysOMe). The nomenclature used to identify the different structural isomers is based on that described previously for other IRMPD studies of metal–amino acid complexes.^{35–37} Briefly, conformations are identified by their metal binding site in brackets, followed by a description of the amino acid orientation by a series of dihedral angles. The angles are denoted as “*c*” (*cis*) for angles < 50°, “*g*” (*gauche*) for angles between 50° and 135° along with an indication of its sign

(+ or –) when needed, and “*t*” (*trans*) for angles > 135°. For charge-solvated (CS) structures, these dihedral angles start with the carboxylic acid hydrogen atom (or methyl carbon atom for CysOMe) and proceed along the molecule to the terminal hydrogen of the amino acid side group; ∠HOCC, ∠OCCC, ∠CCCS, and ∠CCSH. The former or latter angles are missing if the carboxylic acid or sulfur has been dehydrogenated, respectively. The deprotonation site is designated by a negative ion symbol on the appropriate atom. In the case of salt-bridge (SB) structures, the proton originally on the carboxylic acid terminus is attached instead to the nitrogen. For these complexes, the first dihedral angle starts at this bridging proton and moves along the molecule as above. In the case of the [M(Cys-H)]⁺ complexes, both the sulfur and carboxylic acid proton sites can participate in deprotonation and salt-bridge formation.

Theoretical results for [M(Cys-H)]⁺. For both metals, the GS is a tridentate [N,CO,S⁻] *tgg* geometry, with deprotonation at the side-chain sulfur, for all levels of theory (Table 1). This is similar to the results of Mori *et al.* who find this [N,CO,S⁻] *tgg* structure as the ground state conformer for [(H₂O)M(Cys-H)]⁺ where M = Zn²⁺ (gas phase and in solution) and Cd²⁺ (gas phase).⁹ As seen in Fig. 1 for [Zn(Cys-H)]⁺ [N,CO,S⁻] *tgg*, the metal is bound to the amino nitrogen, carbonyl oxygen, and sulfur with bond distances of 2.139, 2.141, and 2.215 Å, respectively. For the [Cd(Cys-H)]⁺ GS structure, the bond distances to the metal are elongated by 0.258 Å for N–M, 0.285 Å for CO–M, and 0.190 Å for S–M. The longer bond distances are largely accounted for by the 0.21 Å larger ionic radius of Cd²⁺ compared to Zn²⁺.³⁸ The [N,CO,S⁻] *cgg* conformer is 26 kJ mol⁻¹ higher in 298 K free energy at all levels of theory for both metals because the intramolecular OH⁺OC hydrogen bond is lost. DFT predicts the bidentate species, [N,S⁻] *tgt* and [CO,S⁻] *cgg*, are lower in energy than the tridentate [N,OH,S⁻] *tgg* (where the

Table 1 B3LYP,^a B3P86, and MP2(full) relative free energies (kJ mol⁻¹) at 298 K of low-lying conformers of [M(Cys-H)]⁺ and [M(CysOMe-H)]⁺^b

Complex	Structure	Zn	Cd
[M(Cys-H)] ⁺	[N,CO,S ⁻] <i>tgg</i>	0.0 (0.0), 0.0, 0.0	0.0 (0.0), 0.0, 0.0
	[N,CO,S ⁻] <i>cgg</i>	26.6 (26.2), 26.2, 25.4	25.3 (25.1), 24.8, 26.0
	[CO,S ⁻] <i>cgg</i>	31.4 (36.4), 35.1, 48.7	30.0 (36.3), 32.0, 46.3
	[N,S ⁻] <i>tgt</i>	37.1 (41.4), 44.0, 44.3	26.6 (32.0), 31.6, 36.5
	[CO ⁻ ,S ⁻] <i>cgg^c</i>	40.0 (40.9), 44.5, 46.0	45.6 (47.0), 47.0, 50.7
	[N,OH,S ⁻] <i>tgg</i>	41.4 (39.6), 45.4, 38.4	34.6 (33.4), 38.9, 34.9
	[CO,S ⁻] <i>ctg</i>	53.6 (57.4), 58.0, 71.8	43.0 (47.4), 45.8, 59.4
	[N,CO ⁻ ,S] <i>ggg</i>	62.1 (59.1), 62.3, 59.6	81.6 (78.6), 81.9, 83.8
	[N,S ⁻] <i>cgt</i>	70.3 (73.6), 76.6, 78.0	59.2 (63.5), 63.4, 69.0
	[N ⁻ ,CO,S] <i>tggg</i>	103.6 (104.3), 104.6, 105.9	105.8 (106.7), 107.9, 113.9
	[S ⁻] <i>tgg</i>	155.3 (162.2), 175.8, 191.4	85.3 (94.2), 99.8, 106.9
	[M(CysOMe-H)] ⁺	[N,CO,S ⁻] <i>tgg</i>	0.0 (0.0), 0.0, 0.0
[N,CO,S ⁻] <i>cgg</i>		35.9 (33.1), 34.8, 35.8	37.5 (34.6), 36.4, 37.9
[N,S ⁻] <i>tgt</i>		41.2 (45.5), 47.6, 50.8	30.6 (35.7), 35.1, 40.9
[N,OMe,S ⁻] <i>tgg</i>		44.8 (40.0), 47.4, 38.3	38.8 (34.6), 41.6, 35.3
[CO,S ⁻] <i>tgg</i>		60.7 (66.4), 69.2, 79.3	55.4 (61.8), 62.0, 74.7
[CO,S ⁻] <i>ctg</i>		79.7 (80.4), 86.2, 96.3	75.1 (76.7), 79.8, 93.3
[N,S ⁻] <i>cgt</i>		87.4 (87.8), 92.6, 95.9	75.6 (76.8), 78.7, 84.6
[N ⁻ ,CO,S] <i>tggg</i>		103.2 (103.5), 104.2, 106.8	105.0 (104.9), 107.1, 113.3

^a Values including empirical dispersion corrections are given in parentheses. ^b Calculations performed at B3LYP, B3P86, and MP2(full) levels of theory using a 6-311+G(2d,2p) basis set for Zn-containing complexes and def2TZVPP for Cd-containing complexes. Geometries and vibrational frequencies calculated at B3LYP/6-311+G(d,p) level for Zn-containing complexes and B3LYP/def2TZVP for Cd-containing complexes. Energies include ZPE corrections scaled by 0.989. ^c Salt-bridge between NH₃⁺, CO₂⁻, and S⁻ groups.

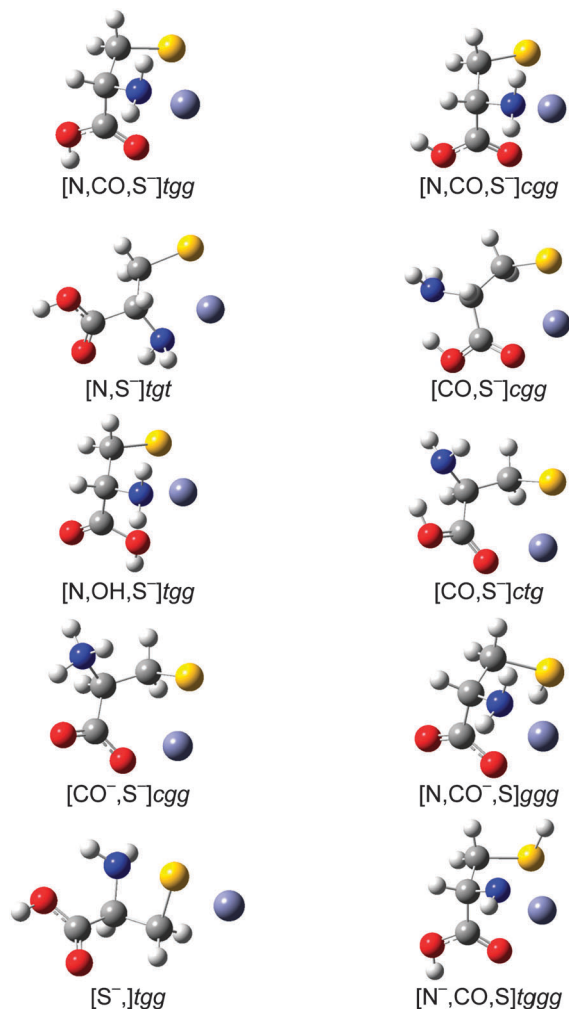


Fig. 1 Structures of select low-lying $[\text{Zn}(\text{Cys-H})]^+$ complexes calculated at the B3LYP/6-311+G(d,p) level of theory. Grey = C, red = O, blue = N, yellow = S, white = H, light purple = Zn.

hydroxyl group is bound to the metal rather than the carbonyl), whereas MP2(full) inverts this order and places $[\text{N,OH,S}^-]tgg$ as the lowest energy and $[\text{CO,S}^-]cgg$ as the highest energy of these three conformers. All levels of theory predict that both metals have similar relative energetics for the $[\text{CO,S}^-]cgg$ species (Cd being more stable by 1–3 kJ mol^{-1}). The $[\text{N,OH,S}^-]tgg$ species have Cd complexes more stable by 3–7 kJ mol^{-1} , and the $[\text{N,S}^-]tgt$ conformer (as well as its *cgt* variant) is more stable by about 10 kJ mol^{-1} for Cd than for Zn. These differences are probably related to the five-membered rings in the latter complexes (Fig. 1), which are stabilized for Cd^{2+} because the longer N–M and S–M bond distances relieve torsional strain in these rings.

Deprotonation is also possible at the carboxylic acid or amine groups. For $[\text{M}(\text{Cys-H})]^+$, the lowest energy conformer with deprotonation at the carboxylic acid is the salt-bridge $[\text{CO}^-,\text{S}^-]cgg$ lying 40–46 kJ mol^{-1} above the GS for Zn^{2+} and 46–51 kJ mol^{-1} for Cd^{2+} . This is lower than $[\text{N,OH,S}^-]tgg$ and $[\text{CO,S}^-]ctg$ for Zn^{2+} but not for Cd^{2+} . The tridentate $[\text{N,CO}^-,\text{S}^-]ggg$ lies another 13–22 kJ mol^{-1} higher for Zn^{2+} and

26–35 kJ mol^{-1} higher for Cd^{2+} . Deprotonation at N is much less favorable with $[\text{N}^-,\text{CO,S}]tggg$ calculated to be 104–114 kJ mol^{-1} higher in 298 K free energy for both metals.

In general, the two DFT levels of theory predict the same trends in relative energy with the exception of $[\text{N,CO}^-,\text{S}]ggg$, Table 1; whereas B3LYP-GD3BJ and MP2(full) levels greatly favor tridentate conformations compared to the bidentate species. There is reasonable agreement among all levels of theory (deviations less than 10 kJ mol^{-1}) for the relative free energies of most conformers, Table 1. The two $[\text{CO,S}^-]$ conformers show larger deviations with MP2(full) results lying 16–18 kJ mol^{-1} above the B3LYP values (with B3P86 and B3LYP-GD3BJ being slightly higher). The biggest differences occur for the extended $[\text{S}^-]tgg$ structure, with deviations of 22–36 kJ mol^{-1} . Here also, changing the metal drastically alters the relative energies with Zn^{2+} being much higher in relative energy. Here the stability appears to be related to the strength of the S–N bond (forming a four-membered ring, Fig. 1). For the Cd complex, this intermolecular S–N bond distance is 0.151 Å shorter than that calculated for the Zn^{2+} complex (2.295 Å), suggesting more covalent character in the former.

Theoretical results for $[\text{M}(\text{CysOMe-H})]^+$. Theory predicts similar low energy structures for the substituted amino acid complexes, $[\text{M}(\text{CysOMe-H})]^+$, as compared to $[\text{M}(\text{Cys-H})]^+$. Relative 298 K free energies for $[\text{M}(\text{CysOMe-H})]^+$ can be found in Table 1 (with 0 K values in Table S1 of the ESI†). As for Cys, the predicted lowest energy structure for the metal binding to CysOMe is the tridentate coordination, $[\text{N,CO,S}^-]tgg$, with deprotonation at the thiol. In these GSs, the exchange of the carboxylic acid hydrogen for a methyl shortens the O–M bond distances by 0.028 Å for the Zn^{2+} complex and 0.027 Å for Cd^{2+} . Clearly, methylation eliminates structures associated with deprotonation of the carboxylic acid and also pushes the $[\text{N,CO,S}^-]cgg$ structure to higher energy (now 36 kJ mol^{-1} above the *tgg* ground structure). Presumably, this occurs because of unfavorable interactions between the methyl group and the amino acid backbone. Indeed, most structures for the $[\text{M}(\text{CysOMe-H})]^+$ complexes have relative energies that are higher than those for the $[\text{M}(\text{Cys-H})]^+$ analogues. This is most apparent in the $[\text{CO,S}^-]$ conformers with the deprotonated CysOMe lying 23–34 kJ mol^{-1} higher in relative energy compared to their Cys analogs. Exceptions to this general trend are the $[\text{N,OMe,S}^-]tgg$ and $[\text{N}^-,\text{CO,S}]tggg$ structures, where the relative energies compared to their $[\text{M}(\text{Cys-H})]^+$ counterparts are essentially equivalent for CysOMe (lower by <1 kJ mol^{-1}) at the MP2(full) level.

Theoretical results for $\text{CdCl}^+(\text{CysOMe})$. For the intact CysOMe binding with CdCl^+ , the predicted GS is again tridentate $[\text{N,CO,S}]tggg_+$, which is the direct analogue of the GS for deprotonated Cys and CysOMe (Tables 1 and 2). The $[\text{N,CO,S}]tggg_-$ conformer is only ~2 kJ mol^{-1} higher in 298 K free energy at all levels of theory and differs in structure from the GS only in the orientation of the SH hydrogen. These structures are similar to the GSs found in previous work for $\text{H}^+(\text{Cys})$,³⁹ $\text{M}^+(\text{Cys})$ where $\text{M} = \text{Li}$ and Na ,²⁰ as well as predictions by Russo *et al.* of $\text{M}^{2+}(\text{Cys})$ where $\text{M} = \text{Cu}$, Zn , Cd and Hg .⁸ Previous theoretical work in the Armentrout group has found that the CS structures

Table 2 Relative free energies (kJ mol⁻¹) at 298 K of low-lying CdCl⁺(CysOMe) conformers^a

Structure	B3LYP ^b	B3P86	MP2(full)
[N,CO,S]tggg ⁺	0.0 (0.0)	0.0	0.0
[N,CO,S]tggg ⁻	2.0 (2.6)	2.1	2.6
[S ⁻]tcg ^c	20.8 (22.3)	21.4	24.8
[N,CO]tgtg ⁻	22.6 (31.8)	27.4	33.6
[N,CO]tggg	23.0 (31.5)	27.6	33.0
[N,CO]tcgg	25.7 (34.7)	30.4	36.3
[N,S]tgtg	27.8 (34.6)	30.3	38.0
[N,CO]tgtg ⁺	28.2 (37.6)	33.1	39.7
[CO,S ⁻]ttg ^c	28.5 (32.6)	29.2	33.4
[N,OMe,S]tggg ⁺	29.7 (34.3)	30.7	23.5
[N,OMe,S]tggg ⁻	34.1 (29.6)	35.4	28.6
[N,CO,S]cggg	40.6 (37.9)	39.7	41.0
[CO,S]ttgt	58.3 (67.9)	64.2	80.0
[CO,S ⁻]cggg ^c	69.7 (70.3)	68.2	75.7
[CO,S]ctgt	87.6 (93.9)	92.7	109.3

^a Calculations performed at the stated level of theory using a 6-311+G(2d,2p) basis set for Zn-containing complexes and def2TZVPP for Cd-containing complexes. Geometries and vibrational frequencies calculated at B3LYP/6-311+G(d,p) level for Zn-containing complexes and B3LYP/def2TZVPP for Cd-containing complexes. Energies include ZPE corrections scaled by 0.989. ^b Values including empirical dispersion corrections are given in parentheses. ^c Salt-bridge between NH₃⁺, CO₂⁻, and S⁻ groups.

for protonated and metal cationized Cys are highly favored over salt-bridge structures.^{20,36,39} It is worth noting that the lowest energy salt-bridge structure for CdCl⁺(CysOMe) is [S⁻]tcg. This conformer is considerably lower in relative energy at 21–25 kJ mol⁻¹ than the similar structure for the [Cd(Cys-H)]⁺ system at 85–107 kJ mol⁻¹. Similar to the [Cd(CysOMe-H)]⁺ complex, the tridentate [N,CO,S]cggg structure is higher in relative energy by ~40 kJ mol⁻¹.

IRMPD action spectroscopy

Fig. 2 shows the photodissociation spectra of [Zn(Cys-H)]⁺ and [Cd(Cys-H)]⁺ were examined from 550 to 1800 cm⁻¹; whereas [Zn(CysOMe-H)]⁺, [Cd(CysOMe-H)]⁺, and CdCl⁺(CysOMe) were examined from 950 to 1800 cm⁻¹. The lower energy wavelength range was not examined for the latter species because theory suggested there would be little diagnostic information in this region. Dominant dissociation pathways are as follows. Photodissociation of [Zn(Cys-H)]⁺ resulted in the loss of (H₂O + CO). Likewise [Zn(CysOMe-H)]⁺ dissociates by loss of (CH₃OH + CO). [Cd(Cys-H)]⁺ and [Cd(CysOMe-H)]⁺ also dissociate similarly to each other by loss of neutral Cd resulting in formation of the radical cations (Cys-H)⁺ and (CysOMe-H)⁺, respectively. For CdCl⁺(CysOMe), the photodissociation pathway corresponded to the loss of NH₃. The IRMPD action spectra shown correspond to the fractional yield of the product ions as a function of free electron laser wavenumber.

Comparison of the IRMPD spectra in Fig. 2 shows the similarities between the spectra of Zn and Cd containing species for both amino acid analogues. The experimental bands are identified on the basis of previous work^{36,40} as well as comparisons to theoretical spectra. The vertical lines drawn through the spectra at 630, 1020, 1160, 1580, and 1660 cm⁻¹ mark the major bands in the [Zn(Cys-H)]⁺ spectrum. Additional lines at

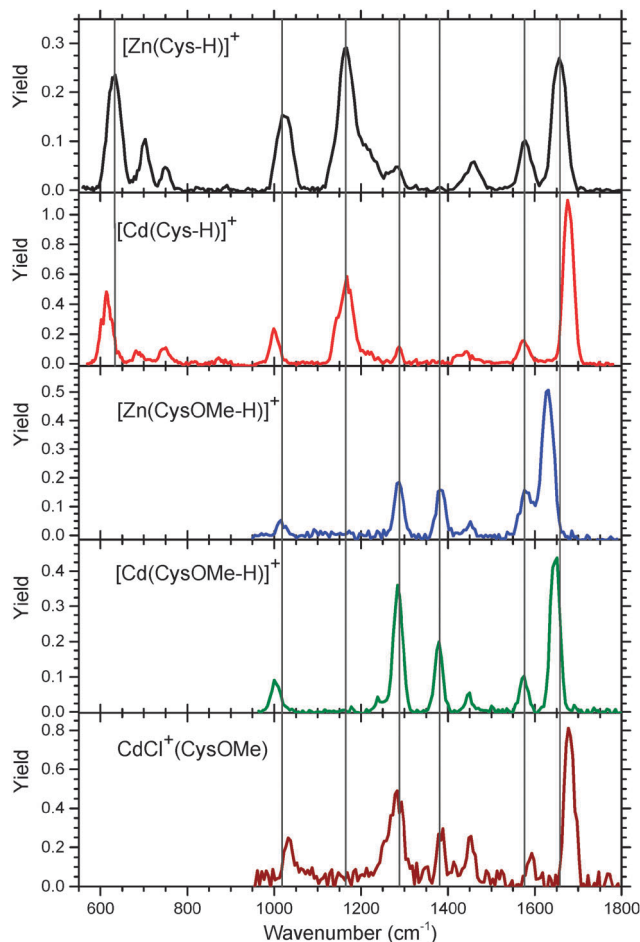


Fig. 2 IRMPD spectra of [Zn(Cys-H)]⁺, [Cd(Cys-H)]⁺, [Zn(CysOMe-H)]⁺, [Cd(CysOMe-H)]⁺ and CdCl⁺(CysOMe) complexes. Solid lines at 630, 1020, 1160, 1280, 1380, 1580 and 1660 cm⁻¹ are drawn to approximate COH wagging, NH₂ wagging, COH bending, HNCH bend, CH₂ umbrella, NH₂ bending and C=O stretch of [Zn(Cys-H)]⁺, respectively.

1280 and 1380 cm⁻¹ mark bands found in the methyl ester spectra. With [Zn(Cys-H)]⁺ as the standard, the major band at 1660 cm⁻¹, the C=O stretch, shifts to the blue for [Cd(Cys-H)]⁺ and CdCl⁺(CysOMe), but shifts to the red for [M(CysOMe-H)]⁺. In all cases, these C=O stretches occur in a lower frequency range than previously observed for alkali metal cationized Cys, 1718 cm⁻¹ for Li⁺(Cys) to 1745 cm⁻¹ for Cs⁺(Cys).³⁶ Clearly, interaction with the doubly charged metal (or nearly doubly charged for CdCl⁺) weakens the CO bond more than the singly charged metal cations. The band at 1580 cm⁻¹, the NH₂ bend, shifts little in most spectra, but shifts to the blue for CdCl⁺(CysOMe). This spectrum also shows a blue shift for the 1020 cm⁻¹ band, associated with NH₂ wagging.

The 610 and 1160 cm⁻¹ bands are attributed to COH wagging and COH bending, respectively. Thus, these bands are not expected to be observed in the cysteine methyl ester complexes as the methyl caps the carboxylic acid terminus of the amino acid, as found for the latter band. Conversely, the presence of these bands in the [M(Cys-H)]⁺ spectra shows that deprotonation of Cys has not occurred at the carboxylic acid.

The other pronounced difference between the amino acid derivatives is the appearance of the 1380 cm^{-1} band in the three CysOMe spectra, which is primarily associated with the methyl umbrella motion. The band at 1280 cm^{-1} corresponds to an HNCH bend, but also has contributions from methyl umbrella motions. The latter explains why the intensity of this band is enhanced in the spectra involving CysOMe.

Comparison to theory: $[\text{M}(\text{Cys-H})]^+$. Fig. 3 shows the experimental $[\text{Zn}(\text{Cys-H})]^+$ IRMPD action spectrum compared to calculated linear IR absorption spectra for selected low energy structures, with corresponding relative 298 K free energies at B3LYP, B3P86, and MP2(full) levels. Although the relative intensities of linear absorption spectra offer good qualitative comparison to the experimental intensities, IRMPD intensities are not always reproduced by the single photon linear absorption spectra. Nonetheless, the major and minor bands predicted by the $[\text{N},\text{CO},\text{S}^-]tgg$ GS conformer correspond well with the observed spectrum, in terms of both band positions and relative intensities. A notable exception is the NH_2 bend observed at 1580 cm^{-1} , but predicted to occur at 1606 cm^{-1} . This vibrational mode is known to have strong anharmonic character in amino acids, an effect that is often manifested as a shift in IRMPD spectra.^{41–43} None of the other

conformers shown in Fig. 3 have predicted spectra that match the experimental spectrum.

The band observed at 1656 cm^{-1} corresponds to the carbonyl stretch, which explains its large intensity. The interaction with the metal cation results in a large shift to the red of the $\text{C}=\text{O}$ stretch band with respect to free Cys, calculated at 1799 cm^{-1} .²⁰ The $\text{C}=\text{O}$ stretch predicted by the ground $[\text{N},\text{CO},\text{S}^-]tgg$ conformer at 1658 cm^{-1} agrees well with the experimental band. The location of the $\text{C}=\text{O}$ stretch in the calculated spectra of the higher energy deprotonated sulfur structures are within 60 cm^{-1} of the observed band, with the exception of $[\text{N},\text{S}^-]$ ($+113\text{ cm}^{-1}$). Nevertheless, the $[\text{N},\text{CO},\text{S}^-]tgg$ ground structure best replicates the $\text{C}=\text{O}$ stretch frequency. The alternative carboxylic acid hydrogen orientation conformer, $[\text{N},\text{CO},\text{S}^-]cgg$, lacks hydrogen bonding within the carboxylic acid, which affects spectral characteristics within the lower frequency range such that the spectrum for this conformer disagrees with experiment. The salt-bridge $[\text{CO}^-,\text{S}^-]cgg$ conformer with a $\text{C}=\text{O}$ stretch at 1716 cm^{-1} does not match experiment, which also does not exhibit the intense band at 1419 cm^{-1} associated with the NH_3 umbrella motion characteristic of this SB conformer. Although the two bidentate species, $[\text{CO},\text{S}^-]cgg$ and $[\text{N},\text{S}^-]tgt$, are also

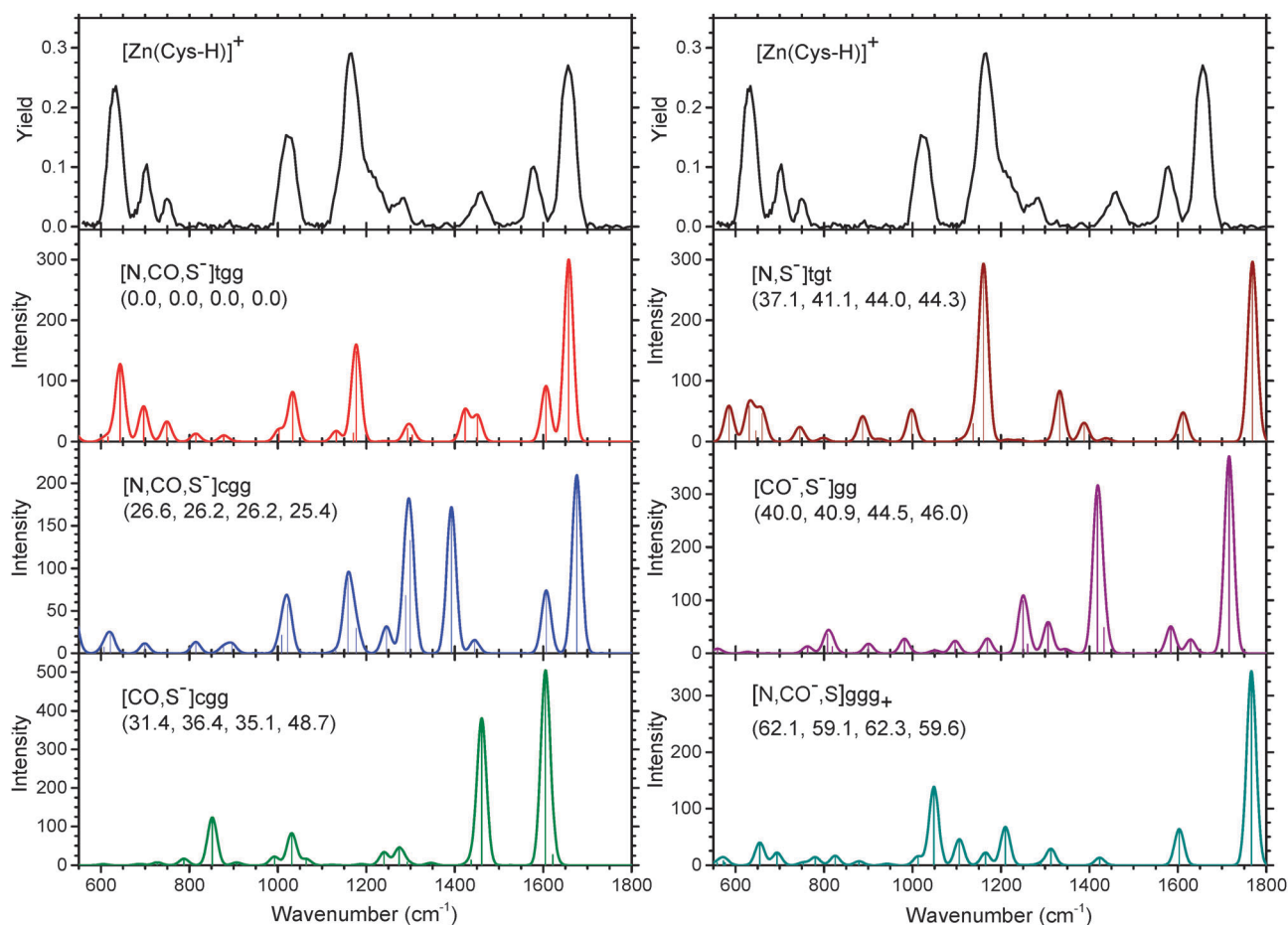


Fig. 3 Comparison of the experimental IRMPD spectrum of $[\text{Zn}(\text{Cys-H})]^+$ with IR spectra of select low-energy conformers predicted at B3LYP/6-311+G(d,p) level. Relative 298 K free energies from Table 1 are given in parentheses calculated at the B3LYP, B3LYP-GD3BJ, B3P86 and MP2(full) levels with 6-311+G(2d,2p) basis set.

deprotonated at the sulfur, their calculated C=O stretch frequencies do not replicate this band observed in the experimental IR action spectrum.

The bands observed at 1167 and 1016 cm^{-1} are also diagnostic bands for the $[\text{N},\text{CO},\text{S}^-]$ structures. These bands are primarily associated with bending of the COH group and the NH_2 wagging motion, respectively. The predicted IR spectra for these conformers adequately reproduce the position and relative intensity of these bands, whereas no other conformation does so at both of these frequencies. In the case of $[\text{N},\text{CO},\text{S}^-]_{cgg}$, this calculated spectrum disagrees with the observed action spectrum by the presence of strong bands calculated at 1296 and 1392 cm^{-1} . Less intense peaks observed at 1461, 750, 703, and 633 cm^{-1} are well represented by the spectrum calculated for the ground conformer. The band at 1461 cm^{-1} corresponds to HCH bends in the amino acid side chain, whereas those observed at 750, 703, and 633 cm^{-1} correspond to wagging motions of the carboxylic acid hydrogen atom. The $[\text{N},\text{S}^-]$ conformer also has bands predicted near the observed 1167 and 1016 cm^{-1} bands, but their relative intensities do not agree well nor do the calculated spectra predict the other diagnostic bands observed in the experimental IR action spectrum. Overall, the experimental IRMPD action spectrum can be adequately explained by the calculated spectrum of the ground $[\text{N},\text{CO},\text{S}^-]_{tgg}$ conformer. The only inadequacies in this comparison are the inconsistent relative intensities of the double peak predicted at 1450 cm^{-1} and the absence of the side band observed near 1210 cm^{-1} . The differences in intensities may result from comparing a multiple photon experimental spectrum with the predicted one-photon spectrum. The missing side band could be an overtone of the band at 620 cm^{-1} .

IRMPD action spectra for $[\text{Cd}(\text{Cys-H})]^+$ and $[\text{Zn}(\text{Cys-H})]^+$ are very similar (Fig. 2), exhibiting all of the same characteristic spectral features. The predicted spectrum for the ground conformer of $[\text{Cd}(\text{Cys-H})]^+$, $[\text{N},\text{CO},\text{S}^-]_{tgg}$, shows good agreement with the observed IRMPD spectrum, as seen in Fig. 4. The intense band observed at 1675 cm^{-1} agrees very well with the predicted C=O for the lowest energy conformer at 1679 cm^{-1} . In addition, the major bands observed at 1166, 1001, and 613 cm^{-1} are also reproduced in the predicted spectrum for $[\text{N},\text{CO},\text{S}^-]_{tgg}$. Another diagnostic band that is reproduced well by the ground conformer is the side band observed at 1143 cm^{-1} , a feature that is not predicted for any other conformer. Consistent with the $[\text{Zn}(\text{Cys-H})]^+$ spectrum, there is again a deviation in the position of the observed 1575 cm^{-1} NH_2 bending band compared to 1605 cm^{-1} calculated for the $[\text{Cd}(\text{Cys-H})]^+$ GS.

Compared with $[\text{Zn}(\text{Cys-H})]^+$, the C=O stretch is calculated to shift to the blue by 20 cm^{-1} and is observed to shift by 27 cm^{-1} upon substitution of Cd for Zn. Likewise, theory and experiment agree that peaks associated with NH_2 and carboxylic acid wagging motions should shift to the blue by 30 and 20 cm^{-1} , respectively, upon Cd substitution.

Comparison to theory: $[\text{M}(\text{CysOMe-H})]^+$. There is good agreement comparing the experimental spectrum of $[\text{Zn}(\text{CysOMe-H})]^+$ to the predicted ground structure, $[\text{N},\text{CO},\text{S}^-]_{tgg}$ (Fig. 5a). Relative intensities and peak positions discussed above are

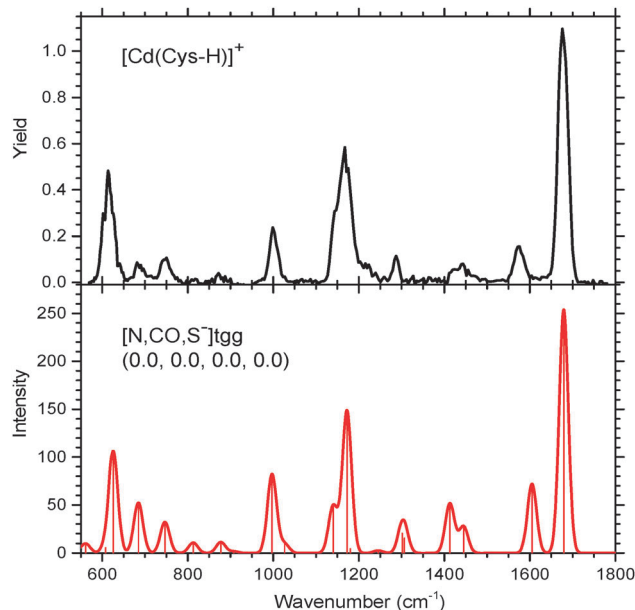


Fig. 4 Comparison of the experimental IRMPD spectrum of $[\text{Cd}(\text{Cys-H})]^+$ with IR spectra of ground structure conformer predicted at B3LYP/def2TZVP level. Relative 298 K free energies from Table 1 are given in parentheses calculated at the B3LYP, B3LYP-GD3BJ, B3P86 and MP2(full) levels with def2TZVPP basis set.

also reproduced well, with the only exception being the NH_2 bending motion observed at 1580 cm^{-1} because of its anharmonic character discussed above. This GS is similar to the GS for the $[\text{M}(\text{Cys-H})]^+$ species. The $[\text{M}(\text{CysOMe-H})]^+$ spectra are similar to that of the $[\text{M}(\text{Cys-H})]^+$ complexes as seen in Fig. 2, with the addition of the diagnostic bands characteristic of the methyl addition. Specifically, these are the band associated with the methyl umbrella motion at 1380 cm^{-1} and the enhancement of the HNCH bend band at 1280 cm^{-1} because this also has contributions from methyl umbrella motions. The predicted spectra for the various tridentate $[\text{N},\text{CO},\text{S}^-]$ complexes are nearly indistinguishable. Only the relative energetics and slight red shift of the C=O stretch band in the *cgg* structure ensure the better agreement for the GS *tgg* spectrum. The bidentate complex, $[\text{N},\text{S}^-]_{tgt}$, does not reproduce the experimental spectrum well with a significant C=O blue shift and bands not characteristic of the observed experimental spectrum.

The $[\text{Cd}(\text{CysOMe-H})]^+$ IRMPD action spectrum is similar to that of its Zn equivalent in both peak shape and position (Fig. 5b). The prominent exceptions are the enlarged gap between the C=O stretch at 1650 cm^{-1} and the NH_2 bend at 1575 cm^{-1} , and the relative intensities of the 1280 and 1380 cm^{-1} peaks. The gap and relative intensities observed experimentally are well reproduced by the predicted GS spectra of the $[\text{N},\text{CO},\text{S}^-]_{tgg}$ complexes. An interesting difference between the Cd and Zn containing complexes is that the 1240 cm^{-1} shoulder predicted in the GS for both species is only observed in the $[\text{Cd}(\text{CysOMe-H})]^+$ IRMPD action spectrum. As for the Zn analogue, the $[\text{N},\text{CO},\text{S}^-]_{tgg}$ calculated spectrum reproduces all

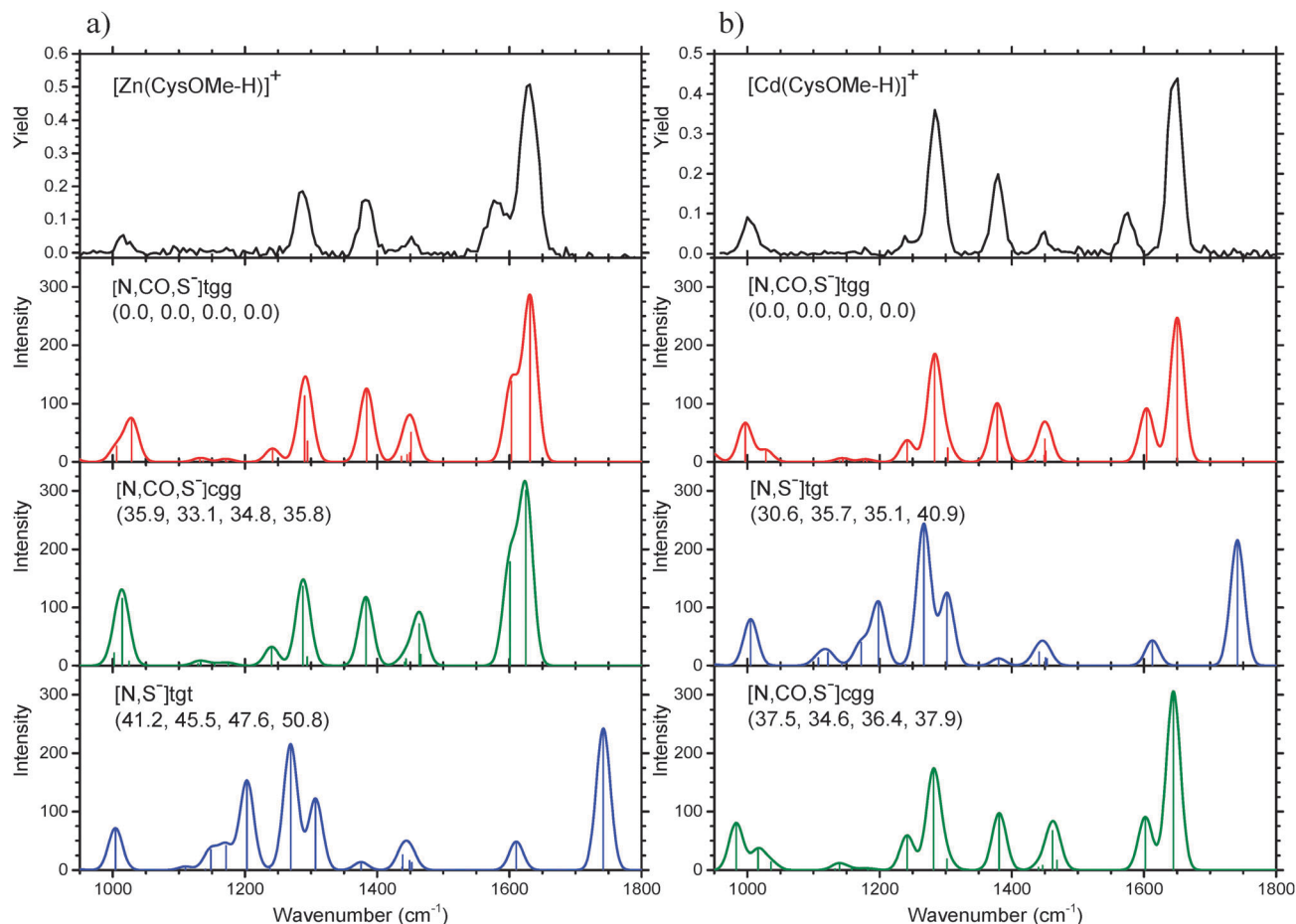


Fig. 5 Comparison of the experimental IRMPD spectrum of (a) $[\text{Zn}(\text{CysOMe-H})]^+$ and (b) $[\text{Cd}(\text{CysOMe-H})]^+$ with calculated IR spectra of select low-energy conformers predicted at B3LYP/6-311+G(d,p) and B3LYP/def2TZVP levels. Relative 298 K free energies from Table 1 are given in parentheses calculated at the B3LYP, B3LYP-GD3BJ, B3P86, and MP2(full) levels with 6-311+G(2d,2p) and def2TZVPP basis sets.

of the bands observed in the experimental spectrum for $[\text{Cd}(\text{CysOMe-H})]^+$ better than those for any higher energy complex.

Comparison to theory: $\text{CdCl}^+(\text{CysOMe})$. Fig. 6 shows the experimental IRMPD action spectrum along with calculated linear IR absorption spectra for selected low-energy structures of $\text{CdCl}^+(\text{CysOMe})$. In analogy with the $[\text{M}(\text{Cys-H})]^+$ and $[\text{M}(\text{CysOMe-H})]^+$ complexes, the predicted ground tridentate $[\text{N,CO,S}]tggg_+$ structure for the intact CysOMe binding to the metal chloride cation is in good agreement with experiment in both peak position and relative intensities. The C=O stretch observed at 1677 cm^{-1} is reproduced well by the predicted band at 1680 cm^{-1} . The only noticeable variation is the predicted NH_2 bend, which is higher in wavenumber by 25 cm^{-1} compared to the observed spectrum, again because of the anharmonicity of this motion. The alternative $[\text{N,CO,S}]tggg_-$ structure has a predicted spectrum nearly identical to that of the $tggg_+$ GS, which is reasonable as the only difference between the two is the direction that the SH hydrogen points. Because this species is very low in energy, it is probably populated in our ion source. At 298 K, its equilibrium population is calculated as 26–31%.

Comparison of the observed spectrum with that predicted for the lowest energy salt-bridge complex, $[\text{S}^-]tgc$, confirms

there are no SB spectral characteristics in the $\text{CdCl}^+(\text{CysOMe})$ system. Again, the most diagnostic band is the C=O stretch, which is predicted to lie much higher in wavenumber than observed. Likewise the strong band predicted at 1430 cm^{-1} is not found experimentally. Although the bidentate $[\text{N,CO}]tg_tg_-$ conformer has peaks in the 1370 and 1450 cm^{-1} range comparable to the observed spectrum, the C=O band is shifted to lower wavenumber and peaks observed in the lower frequency region do not agree with experiment. In addition, the calculated spectrum for the other bidentate binding mode, $[\text{N,S}]tctg$ (not shown), does not reproduce experiment well with a significantly blue shifted C=O stretch and a predicted band at 1213 cm^{-1} that is not observed.

The $\text{CdCl}^+(\text{CysOMe})$ spectrum is similar to that of $[\text{Cd}(\text{CysOMe-H})]^+$ (Fig. 2) with respect to peak intensities and even relative intensities of the diagnostic bands. Notable differences are the blue shifts in bands at 999 to 1032 cm^{-1} , 1575 to 1592 cm^{-1} , and 1650 to 1677 cm^{-1} . These shifts are most likely a result of the presence of the spectator Cl^- ion bound to Cd^{2+} , lengthening the coordinating distance of the metal from the CysOMe binding sites. This difference for the metal to OC is calculated to be 0.02 \AA . Changes in the S–M bond distances are

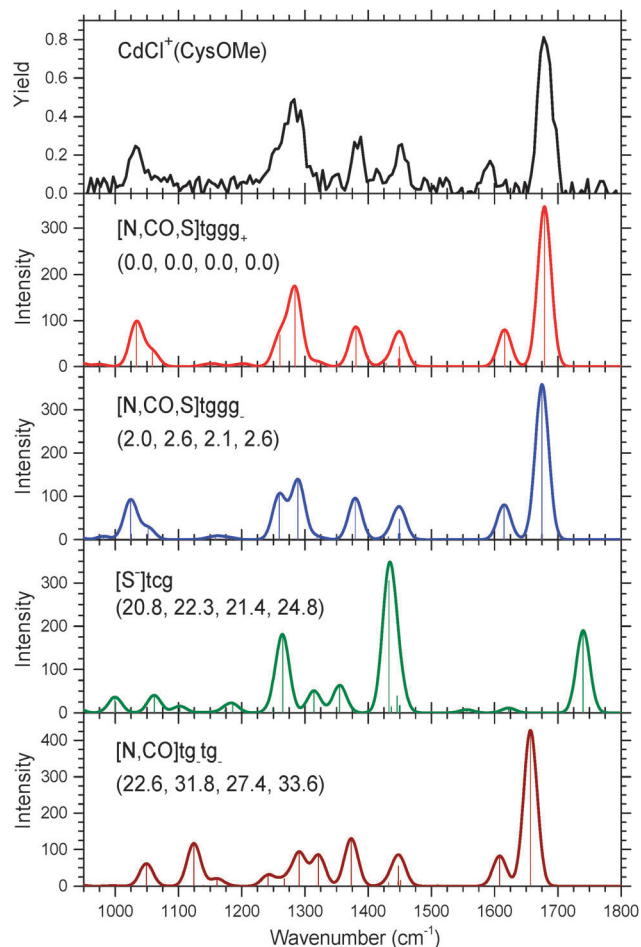


Fig. 6 Comparison of the experimental IRMPD action spectrum of $\text{CdCl}^+(\text{CysOMe})$ with IR spectra of selected low energy conformers predicted at B3LYP/def2TZVP level. Relative 298 K free energies from Table 2 are given in parentheses calculated at the B3LYP, B3LYP-GD3BJ, B3P86 and MP2(full) levels with def2TZVPP basis set.

much more pronounced with that for the CdCl^+ complex longer by 0.36 \AA , clearly because the sulfur group is no longer negatively charged. Interestingly, the peak positions of the C=O stretches for $\text{CdCl}^+(\text{CysOMe})$ and $[\text{Cd}(\text{Cys-H})]^+$ are observed to be very close, consistent with nearly identical Cd to OC binding distances. Compared with the Zn complexes, the C=O stretches for Cd containing species are systematically higher in wavenumber as a result of the larger ionic radius, which elongates the O–M bond lengths, weakens the bond strengths, and decreases the perturbations on the C=O stretch.

Conclusions

IRMPD action spectra in tandem with quantum chemical calculations were used to investigate the role of metal dependence in the structural binding to cysteine and cysteine methyl ester. Action spectra were collected for complexes of Zn^{2+} and Cd^{2+} with deprotonated cysteine and deprotonated cysteine methyl ester, in addition to CdCl^+ with intact cysteine methyl ester. Comparison of these experimental spectra with calculated

IR spectra at the B3LYP/6-311+G(d,p) and B3LYP/def2TZVP levels of theory allow the conformations likely to be present in the experiment to be identified. The deprotonated species are unambiguously identified as charge solvated, tridentate complexes that bind the metal dications to the amine and carbonyl groups of the amino acid backbone and the deprotonated thiol of the side chain. This assignment is in agreement with the predicted ground structures, $[\text{N,CO,S}^-]\text{tgg}$, of these complexes. The assignment of the deprotonation at the thiol site is evident from the positions of the intense C=O stretch bands and the presence of the free OH motion of the intense COH bend band observed in the cysteine systems. The excellent agreement between the Cys and CysOMe observed spectra corroborates thiol deprotonation for the cysteine systems. The comparison of experiment and theory finds $\text{CdCl}^+(\text{CysOMe})$ to bind in an analogous fashion, $[\text{N,CO,S}^-]\text{tggg}^+$. Thus, the presence of the Cl^- spectator ion has little effect on the observed spectra or predicted low energy conformer.

The action spectra are very similar for both Zn^{2+} and Cd^{2+} complexed with the amino acids. Minor differences in the positions and relative intensities were observed, most notably at the position of the C=O stretch and NH_2 wagging bands. These differences are also predicted and observed in the IR spectra for the ground complexes and all spectral characteristics were well reproduced by the calculated ground structures. Examination of the GS structures indicates that zinc binds more tightly than cadmium to Cys and CysOMe. This is evident from the differences in the metal to binding site bond distances, which are $>0.2 \text{ \AA}$ larger for Cd^{2+} . This difference is consistent with the difference in ionic radii, 0.78 \AA for Zn^{2+} and 0.99 \AA for Cd^{2+} .³⁸ Upon investigating the role of metal binding to cysteine, significant structural changes in motifs for binding in the metal–cysteine complex do not occur when zinc ion is replaced with the toxic cadmium ion. This similarity presumably allows for facile substitution of Zn by Cd. At this fundamental level, the change in binding site spacing of the M^{2+} to a single Cys residue may lead to the toxic effects of zinc finger deactivation by cadmium. The weaker binding upon zinc replacement by cadmium may lead to misfolding of these metal dependent proteins. In addition, it needs to be considered that zinc finger proteins have a Zn^{2+} metal bound to four amino acid residue ligands, and the additional ligands may be necessary to understand how metal replacement influences structural changes. Nevertheless, the present study provides important insight to begin understanding the involvement of metal dependence within metalloproteins and acts as a valuable first step for future work that tries to mimic physiologically relevant binding sites with additional amino acids.

Acknowledgements

Financial support for this work was provided by the National Science Foundation, Grants CHE-1359769 and PIRE-0730072. The skillful assistance of the FELIX staff is appreciatively acknowledged. Also, we gratefully thank the Center for High

Performance Computing at the University of Utah for their generous allocation of computing time.

Notes and references

- J. M. Berg and Y. Shi, *Science*, 1996, **271**, 1081–1085.
- A. D. Frankel, J. M. Berg and C. O. Pabo, *Proc. Natl. Acad. Sci. U. S. A.*, 1987, **84**, 4841–4845.
- N. P. Pavletich and C. O. Pabo, *Science*, 1991, **252**, 809–817.
- F. W. Sunderman, Jr. and A. M. Barber, *Ann. Clin. Lab. Sci.*, 1988, **18**, 267–288.
- P. F. Predki and B. Sarkar, *J. Biol. Chem.*, 1992, **267**, 5842–5846.
- M. Asmuss, L. H. F. Mullenders, A. Eker and A. Hartwig, *Carcinogenesis*, 2000, **21**, 2097–2104.
- M. Huang, D. Krepkiy, W. W. Hu and D. H. Petering, *J. Inorg. Biochem.*, 2004, **98**, 775–785.
- M. Belcastro, T. Marino, N. Russo and M. Toscano, *J. Mass Spectrom.*, 2005, **40**, 300–306.
- S. Mori, T. Endoh, Y. Yaguchi, Y. Shimizu, T. Kishi and T. K. Yanai, *Theor. Chem. Acc.*, 2011, **130**, 279–297.
- T. E. Cooper, J. T. O'Brien, E. R. Williams and P. B. Armentrout, *J. Phys. Chem. A*, 2010, **114**, 12646–12655.
- T. E. Cooper and P. B. Armentrout, *Chem. Phys. Lett.*, 2010, **486**, 1–6.
- L. Banu, V. Blagojevic and D. K. Bohme, *J. Am. Soc. Mass Spectrom.*, 2013, **24**, 1534–1542.
- T. E. Hofstetter, C. Howder, G. Berden, J. Oomens and P. B. Armentrout, *J. Phys. Chem. B*, 2011, **115**, 12648–12661.
- D. Oepts, A. F. G. van der Meer and P. W. van Amersfoort, *Infrared Phys. Technol.*, 1995, **36**, 297–308.
- N. C. Polfer, J. Oomens, D. T. Moore, G. von Helden, G. Meijer and R. C. Dunbar, *J. Am. Chem. Soc.*, 2006, **128**, 517–525.
- J. J. Valle, J. R. Eyler, J. Oomens, D. T. Moore, A. F. G. van der Meer, G. von Helden, G. Meijer, C. L. Hendrickson, A. G. Marshall and G. T. Blakney, *Rev. Sci. Instrum.*, 2005, **76**, 023103.
- N. C. Polfer and J. Oomens, *Phys. Chem. Chem. Phys.*, 2007, **9**, 3804–3817.
- A. G. Marshall, T. C. L. Wang and T. L. Ricca, *J. Am. Chem. Soc.*, 1985, **107**, 7893–7897.
- S. H. Guan and A. G. Marshall, *Int. J. Mass Spectrom. Ion Processes*, 1996, **158**, 5–37.
- P. B. Armentrout, E. I. Armentrout, A. A. Clark, T. E. Cooper, E. M. S. Stennett and D. R. Carl, *J. Phys. Chem. B*, 2010, **114**, 3927–3937.
- M. J. Frisch, G. W. Trucks, H. B. Schlegel, G. E. Scuseria, M. A. Robb, J. R. Cheeseman, G. Scalmani, V. Barone, B. Mennucci, G. A. Petersson, H. Nakatsuji, M. Caricato, X. Li, H. P. Hratchian, A. F. Izmaylov, J. Bloino, G. Zheng, J. L. Sonnenberg, M. Hada, M. Ehara, K. Toyota, R. Fukuda, J. Hasegawa, M. Ishida, T. Nakajima, Y. Honda, O. Kitao, H. Nakai, T. Vreven, J. A. Montgomery, J. E. Peralta, F. Ogliaro, M. Bearpark, J. J. Heyd, E. Brothers, K. N. Kudin, V. N. Staroverov, R. Kobayashi, J. Normand, K. Raghavachari, A. Rendell, J. C. Burant, J. M. Millam, S. S. Iyengar, J. Tomasi, M. Cossi, N. Rega, J. M. Millam, M. Klene, J. E. Knox, J. B. Cross, V. Bakken, C. Adamo, J. Jaramillo, R. Gomperts, R. E. Stratmann, O. Yazyev, A. J. Austin, R. Cammi, C. Pomelli, J. W. Ochterski, R. L. Martin, K. Morokuma, V. G. Zakrzewski, G. A. Voth, P. Salvador, J. J. Dannenberg, S. Dapprich, A. D. Daniels, O. Farkas, J. B. Foresman, J. V. Ortiz, J. Cioslowski and D. J. Fox, *Gaussian 09, Revision A.02*, Gaussian Inc., Pittsburgh, PA, 2009.
- A. D. Becke, *J. Chem. Phys.*, 1993, **98**, 5648–5652.
- R. Ditchfield, W. J. Hehre and J. A. Pople, *J. Chem. Phys.*, 1971, **54**, 724–728.
- S. Grimme, S. Ehrlich and L. Goerigk, *J. Comput. Chem.*, 2011, **32**, 1456–1465.
- F. Weigend and R. Ahlrichs, *Phys. Chem. Chem. Phys.*, 2005, **7**, 3297–3305.
- D. Andrae, U. Haeussermann, M. Dolg, H. Stoll and H. Preuss, *Theor. Chim. Acta*, 1990, **77**, 123–141.
- K. L. Schuchardt, B. T. Didier, T. Elsethagen, L. Sun, V. Gurumoorthi, J. Chase, J. Li and T. L. Windus, *J. Chem. Inf. Model.*, 2007, **47**, 1045–1052.
- J. P. Perdew, *Phys. Rev. B: Condens. Matter Mater. Phys.*, 1986, **33**, 8822–8824.
- C. Möller and M. S. Plesset, *Phys. Rev.*, 1934, **46**, 618–622.
- M. Citir, C. S. Hinton, J. Oomens, J. D. Steill and P. B. Armentrout, *J. Phys. Chem. A*, 2012, **116**, 1532–1541.
- R. C. Dunbar, J. Steill, N. C. Polfer and J. Oomens, *J. Phys. Chem. B*, 2009, **113**, 10552–10554.
- J. S. Prell, J. T. O'Brien, J. D. Steill, J. Oomens and E. R. Williams, *J. Am. Chem. Soc.*, 2009, **131**, 11442.
- J. T. O'Brien, J. S. Prell, J. D. Steill, J. Oomens and E. R. Williams, *J. Phys. Chem. A*, 2008, **112**, 10823–10830.
- R. C. Dunbar, N. C. Polfer and J. Oomens, *J. Am. Chem. Soc.*, 2007, **129**, 14562–14563.
- A. L. Heaton, V. N. Bowman, J. Oomens, J. D. Steill and P. B. Armentrout, *J. Phys. Chem. A*, 2009, **113**, 5519–5530.
- M. Citir, E. M. S. Stennett, J. Oomens, J. D. Steill, M. T. Rodgers and P. B. Armentrout, *Int. J. Mass Spectrom.*, 2010, **297**, 9–17.
- D. R. Carl, T. E. Cooper, J. Oomens, J. D. Steill and P. B. Armentrout, *Phys. Chem. Chem. Phys.*, 2010, **12**, 3384–3398.
- R. G. Wilson and G. R. Brewer, *Ion Beams with Applications to Ion Implantation*, Wiley, New York, 1973.
- P. B. Armentrout and E. M. S. Stennett, *J. Am. Soc. Mass Spectrom.*, 2014, **25**, 512–523.
- H. Susi, D. M. Byler and W. V. Gerasimowicz, *J. Mol. Struct.*, 1983, **102**, 63–79.
- P. B. Armentrout, M. T. Rodgers, J. Oomens and J. D. Steill, *J. Phys. Chem. A*, 2008, **112**, 2248–2257.
- M. T. Rodgers, P. B. Armentrout, J. Oomens and J. D. Steill, *J. Phys. Chem. A*, 2008, **112**, 2258–2267.
- J. Oomens, D. T. Moore, G. Meijer and G. von Helden, *Phys. Chem. Chem. Phys.*, 2004, **6**, 710–718.